Aleksandra Kowalska, Robert Banasiak, Andrzej Romanowski, Dominik Sankowski
Lodz University of Technology, Institute of Applied Computer Science
Stefanowskiego 18/22, 90-924 Lodz, akowalska@iis.p.lodz.pl

A STUDY OF THE POSSIBILITY OF USING 3D MODELLING AND 3D PRINTING FOR ELECTRICAL CAPACITANCE TOMOGRAPHY SENSOR

Abstract
Nowadays, the optimization of energy consumption and resources is one of the most urgent topics in worldwide industry. The energy consumption monitoring and control in various multiphase flow industrial applications, where a proper flow characteristic and an optimal phase mixture control is crucial, is hard to perform due to the physical and chemical complexity of the processes. The Electrical Capacitance Tomography (ECT) is one of the relatively cheap non-invasive measurement methods that can help in the monitoring and control of optimal energy and resources dozing in industrial processes. ECT diagnostics systems use unique sensors that can non-intrusively detect spatial capacitance changes caused by spatial changes in the electrical permittivity of industrial process components. One of the latest ECT extensions is a three-dimensional measurement strategy that uses a multilayer structure of the capacitance sensor. In this paper, the authors propose a novel approach to the 3D ECT sensors fabrication process that uses 3D computer modelling and 3D printing to easily get any sensor shape, electrode layout, scale and shielding strategy. This study compares the measurement abilities of a 3D ECT sensor fabricated using a traditional hand-made technique with the 3D printed device. The results have proven the potential of the new 3D print-based sensor regarding its significant fabrication time reduction as well as the improvement of the overall 3D ECT sensor measurement accuracy and stability.

Key words
Electrical Capacitance Tomography, 3D printing, industrial processes, optimization, energy, resources

Introduction

Advanced automation and control of production processes play a crucial role in keeping the world economy competitive in their environmental aspect. While costly process equipment and production lines can be seen as the heart of industrial production, modern monitoring and control systems driven by information technology are its brain. They provide the flexibility to adjust production processes quickly in order to achieve efficiency at the lowest possible amount of resources and energy consumption costs. Hence, the development and application of advanced diagnostic systems is one of the most effective levers for immediate and long-term gross energy savings. One of the modern monitoring techniques that can meet these requirements is an electrical process tomography. It is a relatively young imaging method for industrial diagnostics, undergoing dynamic development [1] [2]. Electrical process tomography is now considered an up-to-date method of visualization and it effectively competes with other well-known imaging techniques such as observations of physical-chemical phenomena by using optical cameras or their recording on photographic film. Tomographic imaging allows observation of the structure of the interior of an object without any necessity of interfering or taking an invasive look into its interior. The process of constructing a tomographic image is based on acquiring and processing measuring signals from a sensor or a set of sensors used to study a given object or process. Process tomography offers unique possibilities of visualising industrial processes: structures of solid objects, fluids, gases and multiphase mixtures, as well as the parameters of their flows [3], and, what is more, in real time. The information about the process gained in this manner can be useful for further development of research or as a rich source of knowledge in the field of diagnostics, monitoring and control towards an energy and resource saving. Process tomography systems are those into which theoretical bases, devices [4], algorithms [5] and approaches used in medical tomography are integrated. This can be observed especially in the case of two- and three-dimensional Electrical Impedance Tomography (EIT) and Electrical Resistance Tomography (ERT). These techniques are now acknowledged worldwide as non-invasive visualization methods of rapidly changing physiological processes used for heart or lung diagnostics [6] and solving environmental issues as well [7]. In the case of Electrical Capacitance Tomography (ECT), as opposed to resistance and impedance methods, the measurement itself is fully non-invasive, and we deal with the environment of non-

conductive and typically dielectric properties. Such environments are common in numerous industrial processes. For many years electrical capacitance tomography systems have been regarded as an effective tool for non-invasive diagnosis and monitoring of two-phase, gas-liquid flows, pneumatic conveying of bulk materials in vertical and horizontal pipelines as well as in gravitational transport processes [3][8][9]. Initially capacitance tomography imaging method was used for two-dimensional visualization of an industrial process interior. The acquired measurement data enabled reconstruction of cross-sectional images of the process under test. Such an image allowed one to make only an approximate evaluation of an industrial process state, since the information obtained from measurement data was simplified and applied only to a specific industrial process section. In reality, however, industrial processes are of a spatial nature and require the use of fully three-dimensional imaging technique [10-17] in real-time as well [18]. Main functional components of 3D ECT system have been shown in Fig. 1.

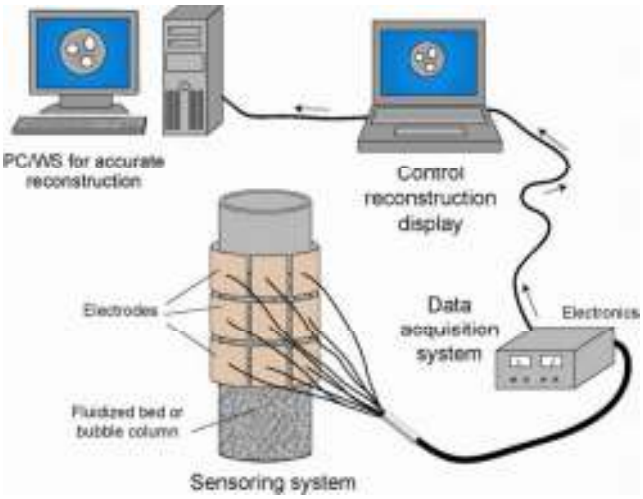

Fig. 1. Example 3D ECT system diagram and its components.
Source: [2]

In the case of a 3D ECT the basic structure of the sensors and the measurement concept are the same as in a 2D tomography (see Fig 2) [14]. The sensor is composed of a set of electrodes, each with a relatively high area of active surface [16]. The difference lies in their layout. In 2D ECT, with its cross-sectional arrangement of electrodes, some inhomogeneities (i.e. objects) can be difficult to distinguish and properly locate in 3D space as presented in Fig 3-A. 3D capacitances tomography uses a unique extended multilayer sensor structure where capacitance measurements are obtained by exciting electrodes from different layers as well and therefore any inhomogenity under test can affect all the measurements and can be distinguished in the final reconstructed image – Fig 3-B [19][20].

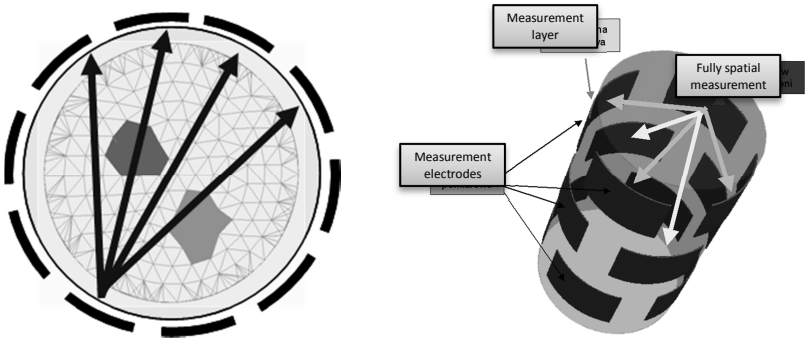

Fig 2. 2D and 3D Tomography.
Source: [19]

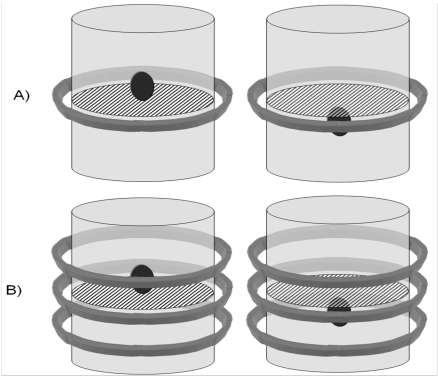

Fig 3. Problem with object location in classic 2D tomography.
Source: [19]

The most common and widely used method of building a 3D ECT sensor is to use a PVC or PMMA pipe and equip it with conductive plates on the outer surface connected with wires. There are two major drawbacks of such an approach. Firstly, a PVC or PMMA pipe has a thickness that can unfavorably reduce an electric field penetration strength. Secondly, manual mounting of these components at specific positions is a sort of "more or less" work and it can bring various disturbances of a proper geometry of sensor structure. An improvement of these issues may be important to a better electric field detection efficiency and may provide more reliable industrial process monitoring and control decision-making – as it is important for energy and resource savings. In this paper, the authors propose a novel approach to the 3D ECT sensor fabrication process that uses 3D computer modelling and 3D printing to easily get any sensor shape, electrode layout, scale and shielding strategy. The proposed solution is a significant step into optimization of a 3D ECT sensor structure and consequently a step into better monitoring efficiency of the industrial process. This study compares the electric field sensing efficiency and measurement abilities of a 3D ECT sensor fabricated using a traditional hand-made technique with the 3D printed device.

3D printing of capacitance sensors

3D printing typically refers to fabrication processes in which various materials are joined or solidified under computer control to create a three-dimensional object. 3D printing is used in both rapid prototyping and additive manufacturing. Objects can be of any shape or any geometry and typically are produced using digital model data from a 3D model or another electronic data source. In an additive process an object is created by putting down successive layers of heated and melted material until the object is completed. Each of these layers can be seen as a thinly sliced horizontal cross-section of the eventual object. In this study, Fused Filament Fabrication technology was used in this research to build a new structure of capacitance sensor. To develop a new mechanical structure of a precise 3D ECT sensor, its computational design has to be prepared as a first. To achieve this goal, a Blender 3D modeller was used for designing a structure of the sensor model and its components. The 3D ECT sensor model has to be designed according to various 3D printing constraints and must be examined for mesh structure errors so that a significant effort has to be put on avoiding very thin walls, redundant mesh points, faces, overhangs, intersections, etc. The mesh model has to be kept as manifold as possible to be 3D printed properly. Blender software is able to generate a 3D sensor output mesh in Stereolithography (STL) format which is widely used 3D printing format. There was a need for splitting a sensor model into two separate symmetric parts due to being limited to a 200mm height of printing. Both parts were redesigned to have special holes and inserts to arrange and connect both parts precisely. The Z-axe outermost electrode layout separation walls and joints have been printed with a half of their thickness to keep it uniform for all 3D ECT sensor model structure. The next step was to prepare 3D printing configuration. In this study the Ultimaker 3 printer with PLA (polylactic acid) printing material and the CURA printing software were used for the building and control of the printing process. The 3D printing solution we used in this research is able to build very precise 3D structures of the ECT sensor with unlimited shapes and wide range of scale. The current maximum resolution of the used printer is 0.4mm for XY axes and 0.06mm for Z axe (print layer thickness) and can be extended by using higher resolution printing modules in the future. The high 3D printing XY resolution was used here to generate very thin sensor wall for keeping distance between electrodes and scanning volume as low as possible. In the past it was very hard or even impossible to achieve in previous classic PMMA (or PVC) pipes-based 3D ECT sensors. Due to the fact that the 3D ECT sensor print model has hanging inter-plane

separation walls the dual printing heads approach has been applied using PVA water-dissolvable material for generating special supports. Finally the printed model was equipped with common electrical elements: electrode plates, wiring and screening system. The main stages of the developed 3D ECT sensors printing workflow have been illustrated in Fig 3.

Fig. 3. The main steps of modelling, design and finishing 3D printed ECT sensor.
Source: Author's

Forward and inverse 3D modelling

The 3D ECT technique is based on measuring the changes in the electric capacitance between the capacitor planes as a result of changes in the dielectric properties of an object under test, located between these planes. The general capacitance tomography measurement concept is as follows: the positive potential on one of the electrodes (excited electrode) is set, while others are grounded. The measured capacitances are collected and then the other electrodes are excited. A limited set of measurements can then be used in image building. The forward problem for 3D electrical capacitance tomography is the simulation of M measurement data for given value of excitation for N electrodes and material permittivity distribution (ε). The main goal of an inverse solution is to approximate of material permittivity distribution (ε) inside of sensor volume using capacitance data C_M and electric field sensitivity matrix S_MxN. This general idea is illustrated in Fig. 4.

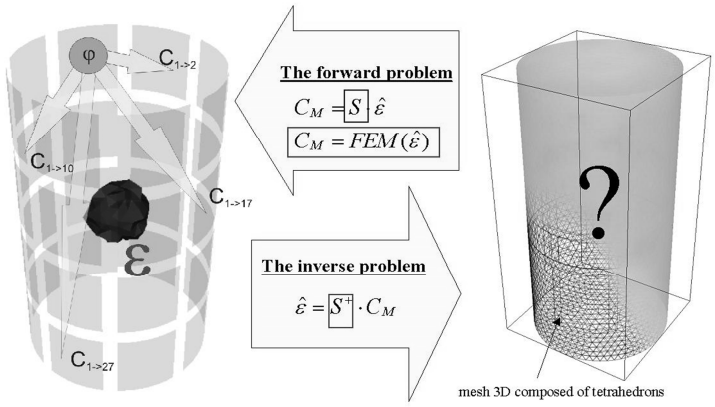

Fig. 4. 3D ECT forward and inverse problem scheme.
Source: Author's

Let's take and assume no internal charges. Then the following equation holds:

$$\nabla \cdot \varepsilon \nabla u = 0 \text{ in } \Omega, \quad (1)$$

where: u is the electric potential, ε is dielectric permittivity and Ω represents the region containing the electric field. The potential on each electrode is known as:

$$u = \nu_k \ \ at \ e_k, \quad (2)$$

where: e_k is the *k*-th electrode held at the potential ν_k. Using the Finite Elements Method we obtain:

$$\mathbf{K}(\varepsilon)\boldsymbol{\varphi} = \mathbf{B}, \quad (3)$$

where: the matrix $\mathbf{K}$ is the discrete representation of the operator $\nabla \cdot \varepsilon \nabla$, the vector **B** is the boundary condition term and $\boldsymbol{\varphi}$ is the vector of electric potential solution. The electric current on the *k*-th electrode e_k is given by:

$$I_k = \int_{e_k} \varepsilon \frac{\delta u}{\delta n} dx^2, (4)$$

where: n is the inward normal on the *k*-th electrode e_k.

To calculate simulated capacitance data, the forward model of the 3D capacitance sensor has to be developed. There are a few ideas of 3D ECT sensor forward modelling [21]. The inverse problem is the imaging result for a given set of measurement data. To solve the inverse problem, we need to find the remedy for the forward problem as a first and to calculate sensitivity maps for the 3D ECT sensor. To obtain a distribution of sensitivity inside the sensor volume, the Fréchet derivative of the measured capacity is calculated in relation to the disturbances that occur in the permeability distribution ε ignoring there by the higher order terms [12] [14].This can simply be extended to a formal proof using operator series and a derivation of sensitivity formula has been given in [6] [12] [14]. In order to obtain a change in the load Q on electrode e_i when e_j is excited, the potential φ_i is applied when electrode e_i is driven and φ_j when e_j is driven [14]. The sensitivity formula can be written as follows:

$$\delta Q_{ij} = \int_{\Omega_p} \delta\varepsilon \nabla\varphi_i \cdot \nabla\varphi_j dx^3, \qquad (5)$$

where: Ω_p represents the capacitance sensor volume perturbed by electrical permittivity distributionε. Here φ_i and φ_j can be calculated by the solution of the forward problem while electrodes e_i and e_j are excited.

Experimental setup

The experimental part of this study was performed entirely in the Process Tomography Research Laboratory at the Institute of Applied Computer Science at the Lodz University of Technology. To compare 3D printed ECT sensor with traditionally made device, the experimental setup consists of two 3D ECT sensors, the Agilent E4980A impedance precision meter and 64-channel computer-controlled multiplexer has been applied. Both sensors were built in accordance with the 3D ECT measurement concept and equipped in 32 electrodes (4 layers with 8 electrodes at each layer). The electrode excitation strategy uses m=496 independent measurement data for n_el without mutual repetitions according to the formula:

$$m = \frac{n_{el}(n_{el}-1)}{2}, \quad (6)$$

Both sensors have two external planes (1st and 4th) and two internal planes (2nd and 3rd). The conventionally-made sensor (we named it: Sensor1) is the sensor we have used in our previous research [9][14]. It was devised and built using the traditional "hand-made" method. The sensor mounting pipe is made of PMMA (polymethyl methacrylate), the sensor total height is 304 mm and its external diameter is 158mm [14]. The mounting pipe thickness is 4mm. Outer electrode layers height is 70mm and inner electrode layers height is 30mm. The electrodes are located on the external surface of the sensor mounting cylinder. The novel sensor (we named it: Sensor2) is based on the 3D modeller design and it was printed using 3D printer [14]. The transparent PLA printing material was used to generate the sensor mechanical structure. Differently from Sensor 1, the outer layers have a height of 40mm of and inner layers have 25mm. The pipe thickness is 0.4mm which is a significant improvement compared to the Sensor 1 structure. It simultaneously assures the insulation of electrodes from industrial process components and keeps the measurement penetration distance and as low as possible. It may have significant positive influence on sensitivity in central area of a sensor. For both sensors, an electrode area and height asymmetry have been applied for outer and inner layers to keep a distant, inter-plane measurement signal detectable by a measurement unit [14].

Fig. 5. The main components of the experimental setup used in this study – a measurement system and two 3D printed test phantoms filled in PE granulate.
Source: Author's

Both sensors structures include a full shielding arrangement including copper-made outer screens and boundary screens. During the measurement, the following strategy was applied: firstly, the sender electrode has a positive potential (5V excitation voltage value has been applied) while the rest of the electrodes are grounded. Each electrode is switched made the sender in turn. [14][24].

Table 1. Experimental Sensor1 and Sensor2 key dimensions and parameters.

	Sensor height [mm]	**Electrode Height [mm]**	**Electrode Width [mm]**	**Total active area [cm^2]**
Sensor1	200	70/30	57	456
Sensor2	130	40/25	55	286

Source: Author's

For the experimental stage, two different experimental permittivity distributions (test1, test2) have been used. The testing phantoms were objects built using 3D printing technique (PLA) and filled in two ways with 3mm PE (polyethylene) granulates. The arrangement of tested phantom has been visualised in Fig 6. The experimental datasets have been normalized using capacitance data for high C_{full} and low C_{empty} uniform permittivity distributions (PE granulate – 3, an air – 1 as a background). In this study the normalization of experimental capacitance data C_n has been calculated according to formula:

$$C_n = \frac{C - C_{empty}}{C_{full} - C_{empty}}, \qquad (7)$$

To compare both sensors a full cycle and the first electrode with the full 31 measurement cycles were taken into consideration.

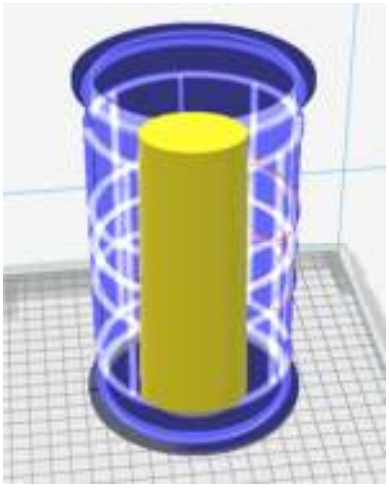

Fig. 6. The arrangement of a tested phantom inside a 3D ECT sensor volume for two options: test1 - a cylinder with 75mm of diameter filled with PE inside; test2 - a cylinder with 75mm of diameter filled with PE outside.
Source: Author's

Results and discussion

In this study we have mainly focused on the of the comparison of detection abilities of Sensor1 and Sensor2 and their responsivity on tested electrical permittivity phantoms test1 and test2. The Sensor1 has already been successfully verified for many industrial applications (two-phase flows, hopper flows) in our laboratory in the past [10]. In this study we treated it as a reference device. The full measurement cycle for test1 object (a PLA printed cylinder filled by PE granulate) and both sensors has been shown in Fig. 7.

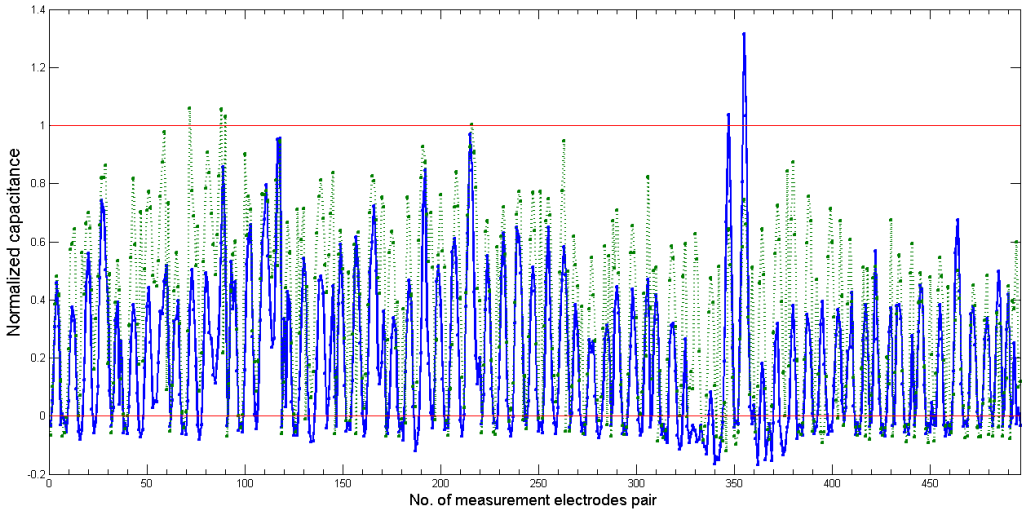

Fig. 7. The full measurement cycle for test1 and Sensor1 – green dotted line, Sensor2 – blue solid line. Red lines determine calibration limits (0;1).
Source: Author's

Both sensors were able to provide reliable calibration data to get stable in time the normalized capacitance vectors. The obtained experimental capacitance data full measurement cycle characteristics for test1 proved the similar abilities of these two devices to detect small objects in the centre of the scanning area. The mean value of the normalized capacitance dataset for Sensor1 is 0.3387 and the standard deviation is 0.3019. The mean value 0.1809 of Sensor2 normalized signal response is lower. This indicates that acquired signal response is weaker.

It points out the slight advantage of Sensor1 over Sensor2. However, the standard deviation is 0.2472, which indicates a better signal stability for Sensor2. We have to keep in mind that Sensor1 has around a 60% larger total area of electrode array in comparison to the 3D printed Sensor2 that surely can provide higher values of electric field intensity inside an investigation area. Fig 8 presents 1st electrode measurement cycle taken from full capacitance data set. This confirms the tendency and comparison results visible for full cycle.

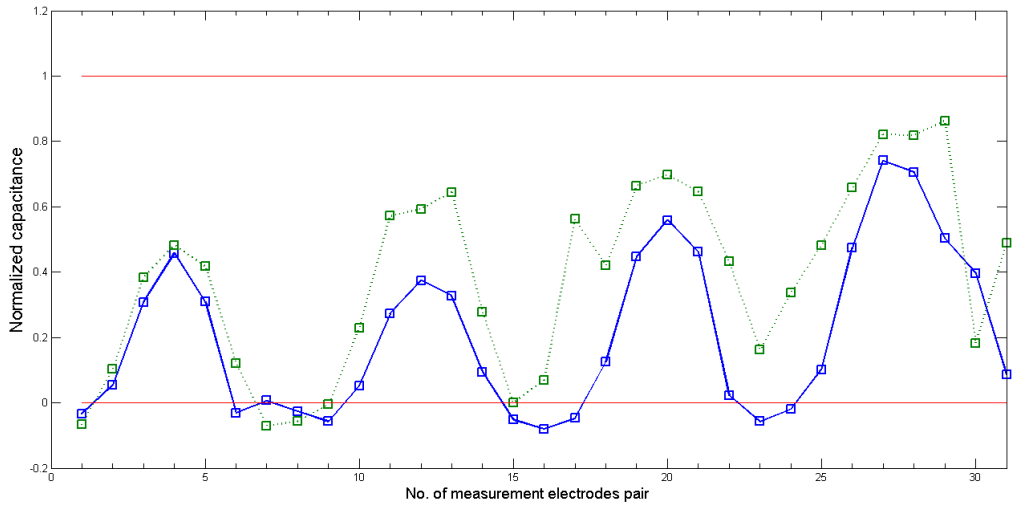

Fig. 8. The 1st electrode measurement cycle (with 2..32) for test1 and Sensor1 – green dotted line, Sensor2 – blue solid line. Red lines determine calibration limits (0;1).
Source: Author's

Test2 investigates the ability of both sensors to detect permittivity distribution close to electrodes array. The full measurement cycle for test2 object (a PLA printed cylinder with an air inside surrounded by PE granulate) and both sensors have been shown in Fig 9. The mean value of normalized capacitance dataset for Sensor1 is

0.5801 and standard deviation is -0.1043. Regarding to test2 we also calculated a standard deviation value for both sensors: Sensor1 - 0.8103 and Sensor2 – 0.4730. This test showed a better performance of Sensor2 comparing to Sensor1 for an object located in the neighbourhood of the electrode array. The signal from Sensor2 better fits calibration limits and is more stable as well. The mean value of Sensor1 is negative (there are few negative normalized capacitance values below -1.5 for the most distant electrode pairs). It can indicate that capacitance measurement for the most distant electrodes is too low to generate positive normalized capacitance data. This confirms some benefits of using 3D printing technology over traditional method.

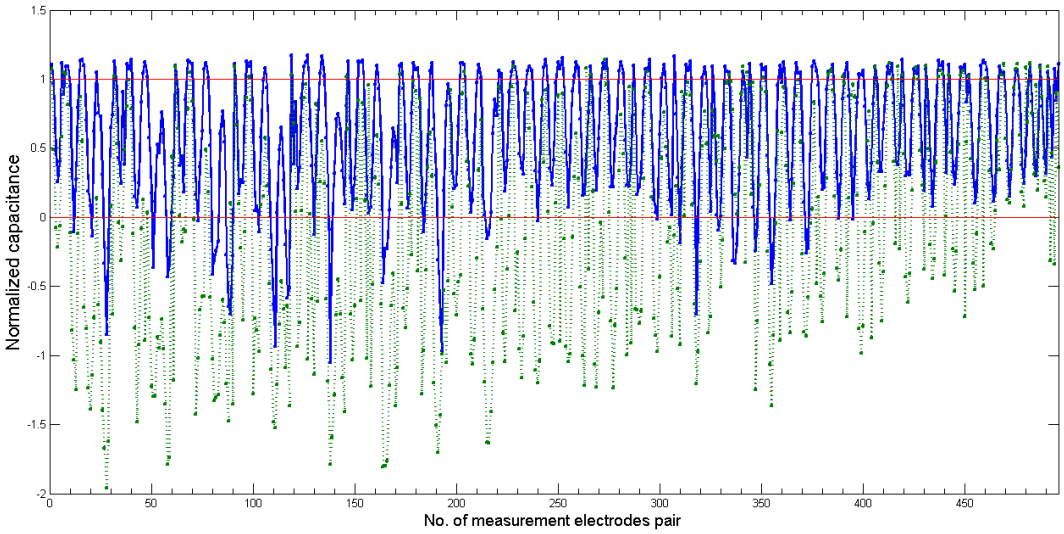

Fig. 9. The full measurement cycle for test2 and Sensor1 – green dotted line, Sensor2 – blue solid line. Red lines determine calibration limits (0;1).
Source: Author's

Fig. 10 presents first electrode measurement cycle graph subtracted from full capacitance data set. The blue line represents 3D printed 3D ECT Sensor2 capacitance data subset for first electrode and the green dotted line represents Sensor1. Capacitance measurement for electrode pair 1-28 is typically the most distant from all of the electrodes array and the hardest to measure due to the limitations of tomography hardware. The new sensor raises this capacitance minimum value to the level that might be acceptable for existing tomography systems [22]. This figure shows the measurement values normalized by means of calibration. It is known that the values should be in the range from 1 to 0 with the accuracy of the amplitude of the noise in the signal. Although neither sensor1 nor sensor2 fall into these values - it can be seen that sensor2 better adapts to the above range.

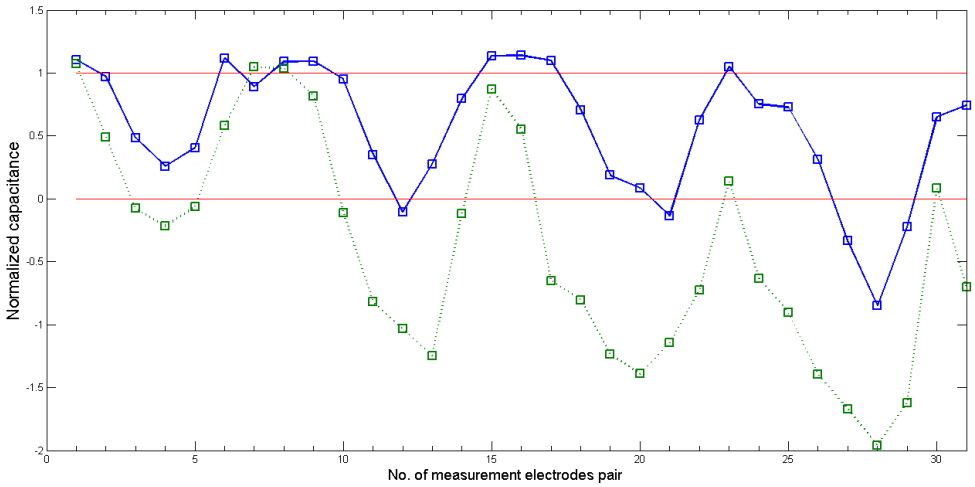

Fig. 10. The first electrode measurement cycle (with 2..32) for test2 and Sensor1 – green dotted line, Sensor2 – blue solid line. Red lines determine calibration limits (0;1).
Source: Author's

Conclusions and future work

In this research work a novel method for high precision design, modelling and build of 3D electrical tomography capacitance sensor was proposed and discussed. A developed solution combines modern 3D printing technique with a knowledge of 3D capacitance imaging and can extend 3D ECT tomography monitoring abilities to an efficiency level inaccessible for process tomography society in the past. The 3D printed ECT sensor advantages over traditionally hand-made made known 3D ECT sensors. It offers very thin wall between electrode array and can be built as a one-piece complex structure that may be easily fitted to industrial process under test. The accuracy of the 3D printed sensor structure is very high due to the reliability, repeatability and high resolution of 3D printing. In this research work, a 3D printed sensor model was compared to a well-known and reliable device used in the previous research. For most tests, we achieved better results of sensor detectability for tested phantoms. The conducted experiments have shown the great potential of using 3D printing technology for making ECT sensors. It seems to be a giant step forward towards high resolution and high precision electrical capacitance tomography systems. The proposed method brings a new era to the ECT sensor making process and now, even the most complex electrode arrays and sensor structures can be easily designed and 3D-printed in a short time. It also drives ECT non-invasive diagnostic technique towards a better and more robust industrial process monitoring and control that can lead to optimize strategy of energy and resources usage. As a future project, some new 3D ECT optimized and complex sensor designs will be tested and developed including: an increasing number of electrodes, changing electrode array shape and screening structures. Another direction could be the design and printing of the 3D ECT sensor optimized and fitted it to a given industrial process that runs in non-circular curved pipes and custom shape tanks or silos. Finally it will be interesting to research on the possible influence of the proposed 3D printing sensor methodology on the efficiency, performance and accuracy of hybrid systems employing contextual data processing or human crowd-computer data processing algorithms [12][21][23].

Acknowledgements

This work was financed by the Lodz University of Technology, Faculty of Electrical, Electronic, Computer and Control Engineering as a part of statutory activity (project no. 501/12-24-1-5418).

References

[1] C.G. Xie, S.M. Huang, C.P. Lenn, A.L. Stoll, M. S. Beck, Experimental evaluation of capacitance tomographic flow imaging systems using physical models, IEE Proc. – Circuits Devices Syst. 141 (1994) 357-368.

[2] A. Pląskowski, M.S. Beck, R. Thorn, T. Dyakowski, Imaging Industrial Flows – Applications of electrical process tomography, IOP Publishing Ltd - Taylor & Francis, 1995.

[3] K. Grudzien, A. Romanowski, D. Sankowski, R.A. Williams, Gravitational Granular Flow Dynamics Study Based on Tomographic Data Processing, Particulate Science and Technology, 26 (2007) 67-82, DOI: 10.1080/02726350701759373

[4] J. Kryszyn, W. T. Smolik, B. Radzik, T. Olszewski, R. Szabatin, Switchless charge-discharge circuit for electrical capacitance tomography, Meas. Sci. Technol., 25 (2014) 115009.

[5] W. Q. Yang, L. Peng, Image reconstruction algorithms for electrical capacitance tomography, Meas. Sci. Technol. 14 (2003) R1–R13.

[6] Ł. Mazurkiewicz, R. Banasiak, R. Wajman, T. Dyakowski, D. Sankowski, Towards 3D Capacitance Tomography, proc. 4th World Congress Industrial Process Tomography, Aizu, 2005, pp. 546-551.

[7] T. Rymarczyk, Using electrical impedance tomography to monitoring flood banks, Int. J. Appl. Electromagn. Mech. 4 (2014) 1–4.

[8] G. Rybak, Z. Chaniecki, K. Grudzień, A. Romanowski, D. Sankowski, Non–invasive methods of industrial processes control, IAPGOS - Informatics, Control. Meas. Econ. Environ. Prot. 4 (2014) 41–45.

[9] I. Jelliti, A. Romanowski, K. Grudzien, Design of crowdsourcing system for analysis of gravitational flow using x-ray visualization, in proc. FedCSIS'16, ACSIS, vol. 8. IEEE, 2016, pp. 1613–1619.

[10] R. Wajman, R. Banasiak, Tunnel-based method of sensitivity matrix calculation for 3D-ECT imaging, Sens. Rev. 34 (2014) 273–283.

[11] Q. Marashdeh, F. Wang, L.S. Fan, W. Warsito, Velocity measurement of multi-phase flows based on electrical capacitance volume tomography, in Proceedings of IEEE Sensors, 2007, pp. 1017–1019.

[12] R. Banasiak, R. Wajman, M. Soleimani, An efficient nodal Jacobian method for 3D electrical capacitance tomography image reconstruction, Insight Non-Destructive Test. Cond. Monit. 51 (2009).

[13] R. Wajman, P. Fiderek, H. Fidos, T. Jaworski, J. Nowakowski, D. Sankowski, R. Banasiak, Metrological evaluation of a 3D electrical capacitance tomography measurement system for two-phase flow fraction determination, Meas. Sci. Technol. 24 (2013) 11, DOI: 10.1088/0957-0233/24/6/065302.

[14] R. Banasiak, R. Wajman, D. Sankowski, M. Soleimani, Three-dimensional nonlinear inversion of electrical capacitance tomography data using a complete sensor model, Progress In Electromagnetics Research PIER, 100 (2010) 219-234.

[15] K. Grudzień, Visualization System for Large-Scale Silo Flow Monitoring Based on ECT Technique, IEEE Sensors Journal. 24 (2017) 8242-8250.

[16] R. Wajman, R. Banasiak, Ł. Mazurkiewicz, T. Dyakowski, D. Sankowski, Spatial imaging with 3D capacitance measurements, Measurement Science and Technology 17 (2006) 2113-2118.

[17] F. Wang, Q. Marashdeh, L.-S. Fan, W. Warsito, A Review: Electrical Capacitance Tomography: Design and Applications, Sensors 10 (2010) 1890-1917.

[18] M. Soleimani, C. N. Mitchell, R. Banasiak, R. Wajman, A. Adler, Four-Dimensional Electrical Capacitance Tomography Imaging Using Experimental Data, Prog. Electromagn. Res. 90 (2009) 171–186.

[19] R. Banasiak, Ł. Mazurkiewicz, R. Wajman, 3D Graphics Hardware and Software Acceleration Features for 3D Tomography, proc.3rd International Symposium on Process Tomography in Poland, Łódź, 2004, pp. 19-23.

[20] R. Banasiak, R. Wajman, Ł. Mazurkiewicz, Study of electrodes layout for three-dimensional electrical capacitance tomography sensors, proc. PROCTOM 2006 - 4th International Symposium on Process Tomography in Poland, Warszawa, 2006, pp. 147-150.

[21] C. Chen, P. Wozniak, A. Romanowski, M. Obaid, T. Jaworski, J. Kucharski, K. Grudzien, S. Zhao, M. Fjeld, Using Crowdsourcing for Scientific Analysis of Industrial Tomographic Images, ACM Trans on Intelligent Systems and Technology 52 (2016) 25.

[22] P. Brzeski, J. Mirkowski, T. Olszewski, A. Pląsowski, W. Smolik, R. Szabatin, Multichannel capacitance tomograph for dynamic process imaging, Opto-Electronics Rev. 11 (2003) 175–180

[23] A. Romanowski, K. Grudzień, P. Woźniak, Contextual processing of ECT measurement information towards detection of process emergency states, In proc. Thirteenth International Conference on Hybrid Intelligent Systems (HIS 2013), Tunis, 2013, pp. 292-298.

[24] R. Banasiak, M. Soleimani, Shape based reconstruction of experimental data in 3D electrical capacitance tomography, NDT & E International, 43 (2010) 241-249.